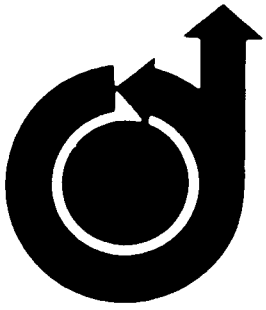

77-188

# Effective Conductivity of Regularly Packed Spheres: Basic Cell Model with Constriction

Y. Ogniewicz, *University of California, Berkeley, Ca.; and* M.M. Yovanovich, *University of Waterloo, Waterloo, Canada*

AIAA 15th AEROSPACE SCIENCES MEETING

Los Angeles, Calif./January 24-26, 1977

# EFFECTIVE CONDUCTIVITY OF REGULARLY PACKED SPHERES: BASIC CELL MODEL WITH CONSTRICTION

Y. Ogniewicz
Graduate Student
University of California, Berkeley

M.M. Yovanovich*
Professor
Thermal Engineering Group
Department of Mechanical Engineering
University of Waterloo
Waterloo, Ontario

## Abstract

Analytical solutions for conduction in basic cells of regularly packed spheres are obtained. The basic cells are shown to consist of a number of effective contact regions. The influence of packing, mechanical load, and gas pressure is determined. Experimental results for a single contact region, and for an FCC basic cell, are in excellent agreement with the analytical results at all mechanical loads and gas pressures for air, argon, and helium.

## Nomenclature

| | |
|---|---|
| $a$ | = contact radius |
| $A$ | = cross-sectional area of a basic cell |
| $D$ | = sphere diameter |
| $E$ | = Young's modulus |
| $F$ | = mechanical load applied upon a basic cell ($P_a A$) |
| $F_1, F_2, F_3$ | = constants defined by Eqs. (23),(24), and (25) |
| $h$ | = height of a basic cell |
| $k_a$ | = apparent conductivity of a basic cell, or of regularly packed spheres |
| $k_e$ | = effective conductivity of a contact region |
| $k_g$ | = local gas conductivity |
| $k_{ge}$ | = effective gaseous conductivity associated with a contact region |
| $k^*_{ge}$ | = non-dimensional effective gaseous conductivity associated with a contact region |
| $k_s$ | = solid conductivity |
| $k_{se}$ | = effective solid conductivity associated with a contact region |
| $L$ | = non-dimensional contact parameter ($D/2a$) |
| $M$ | = modified Knudsen number ($2\alpha\beta\Lambda/D$) |
| $N$ | = normal load on a contact |
| $P$ | = gas pressure |
| $P_a$ | = apparent pressure due to mechanical loading |
| $P_o$ | = standard gas pressure |
| $Pr$ | = Prandtl number |
| $Q_g$ | = total heat flow through the gaseous medium associated with a contact region |
| $r$ | = radial distance from the contact center |
| $R_c$ | = thermal constriction resistance |
| $R_{cr}$ | = thermal constriction region resistance |
| $R_g$ | = thermal resistance of the gaseous medium |
| $R_r$ | = radiation thermal resistance |
| $R_s$ | = thermal resistance of the solid medium |
| $R_t$ | = total resistance of a basic cell |
| $T$ | = mean gas temperature |
| $T_o$ | = standard temperature |
| $\Delta T_a$ | = overall temperature difference of a contact region |
| $x$ | = non-dimensional radial distance ($r/a$) |

### Greek Symbols

| | |
|---|---|
| $\alpha$ | = accommodation factor $[2(2 - \alpha_1)/\alpha_1]$ |
| $\alpha_1$ | = accommodation coefficient |
| $\beta$ | = gaseous parameter $[2\gamma/((\gamma + 1)Pr)]$ |
| $\gamma$ | = ratio of specific heats ($C_p/C_v$) |
| $\delta$ | = local spacing |
| $\delta^*$ | = non-dimensional local spacing ($\delta/a$) |
| $\varepsilon$ | = emissivity |
| $\Delta$ | = quantity defined by $[1/(3P_a(1-\nu^2)/E^{1/3}]$ |
| $\zeta$ | = outer radial limit of the gas region |
| $\zeta^*$ | = non-dimensional outer radial limit of the gas region |
| $\Lambda$ | = mean free path of a gas molecule |
| $\Lambda_o$ | = mean free path of a gas molecule at S.T.P. |
| $\nu$ | = Poisson's ratio |
| $\rho$ | = solid fraction |
| $\sigma$ | = Stefan-Boltzmann constant |

## Introduction

Packed beds have a variety of applications in thermal systems. They provide a large ratio of solid surface area to its volume. This property is useful in application such as catalytic reactors, heat recovery processes, heat exchangers, heat storage systems, etc. Packed spheres are also used as an insulation material, acting as a radiation shield as well as a convection heat flow suppressant, at the expense of an increase of conduction heat transfer.

The heat transfer characteristics of such beds, and particularly the conduction contribution, was the subject matter of a number of studies. The previous work on this subject may be divided among three groups of investigators. The first group [1-4] simplified the analysis by transforming the complex geometry of spherical particles into series and parallel arrangements of macroscopic rectangular volumes of gas and solid. One dimensional heat conduction analysis of such geometry was then performed. When the dependence of the gas conductivity on the Knudsen number was included, it was assumed uniform, and was evaluated at some equivalent spacing obtained from geometry alone. A second group [5-8] has taken the problem further by retaining the actual geometry, i.e., spheres in contact, but the local gas conductivity was assumed uniform over the entire gas region, which actually varies in thickness. In both cases the solid constriction resistances, when incorporated, were

*Associate Fellow AIAA

added in parallel to the other resistances. The third approach [9-10] was to solve the problem numerically. The geometry was retained and the gas conductivity was allowed to vary locally. The numerical solution was relatively successful, although mechanical load and packing were not considered

In the present work, a detailed analysis of individual basic cells representing regularly packed spheres accompanied by experimental results is presented. This approach enables the isolation and analysis of the parameters, namely, mechanical loads, packing, gas pressure and solid gas conductivity ratio. Constriction always occurs when the solid to gas conductivity ratio is relatively large (which is true in most cases). It is obvious that the above condition is necessary for application of this model. The analysis of a single contact region includes the local variation of gas conductivity due to the variable thickness of the gas region, and the bending of the heat flow lines within the solid. A constriction of heat flow into the area in the vicinity of the solid to solid contacts both within the solid and the gas enables one to model the basic cell as an arrangement of thermal resistances associated with contact regions.

## Analysis

### A. Contact Region

Consider two identical spheres in contact as shown in Fig. 1. The two solid surfaces are separated by a gaseous region varying in thickness from zero at the contact to some value, $\delta_o$, at the outer adiabatic boundary Fig. 1. The contact radius is a; the sphere diameter is D. $T_{1a}$ and $T_{2a}$ are temperatures of the two spheres far enough from the contact so as to be assumed relatively uniform. $T_1(r)$ and $T_2(r)$ are the temperature distributions at the solid gas interface. The above is only a particular case of a contact region. The following analysis could be applied to different contact regions such as a sphere-flat contact (which is investigated subsequently), a cylinder-flat contact region, a contact region between a ball bearing and its race, etc.

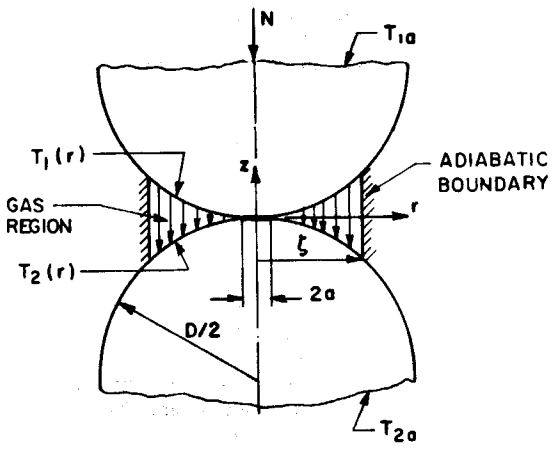


Fig. 1 Contact region between two identical spheres

Heat conduction is assumed to take place through the solid to solid contact region and through the gaseous layer in a parallel configuration. The validity of this assumption has been previously established by other investigators [8,13].

For a relatively small contact to sphere diameter ratio ($2a/D \ll 1$), the constriction resistance is well approximated by that of an isothermal circular contact on a half space, [11] and is given by:

$$R_c = \frac{1}{4k_s a} \tag{1}$$

The contact radius, a, is evaluated by means of the well-known Hertz relation for elastic contacts, which, for two spheres, reduces to:

$$a = [(3/8)ND(1-\nu^2)/E]^{1/3} \tag{2}$$

where N is the normal load, E is Young's modulus, $\nu$ is Poisson's ratio, and D is the diameter of the sphere.

The overall thermal resistance of the solid phase consists of two such constrictions and, hence, is given by:

$$R_s = \frac{1}{2k_s L} \tag{3}$$

where $L = D/2a$. The following result is obtained for the effective solid conductivity, $k_{se}$, defined on the basis of a cube of side D,

$$k_{se} = \frac{k_s}{L} \tag{4}$$

Equation (4) is strictly valid only under vacuum conditions, but, the contribution of the solid conduction to overall conduction diminishes as the gas pressure increases, and hence the error incurred using Eq. (4) when calculating the solid contribution to the overall effective conductivity is small. The thermal resistance of the gaseous phase is defined based on the overall temperature difference (similarly to the solid resistance)

$$R_g = \frac{\Delta T_a}{Q_g} \tag{5}$$

where $\Delta T_a = T_{1a} - T_{2a}$, and $Q_g$ is the total heat flow through the gaseous region.

The heat flow lines in the gaseous region are assumed to be straight and perpendicular to the plane of contact. This assumption is valid in the proximity of the contact where the two solid surfaces are nearly parallel to the contact plane, and it is demonstrated later that the major portion of the gaseous heat transfer occurs through this region. The total heat flow through through the gas is then given by the following integral:

$$Q_g = \int_a^{\zeta} k_g(r) \frac{\Delta T(r)}{\delta(r)} 2\pi r dr \tag{6}$$

where $k_g(r)$ is the local gas conductivity depending upon the local spacing, $\delta(r)$, and the interstitial gas mean free path, $\Lambda$. The local gas conductivity is assumed to be equal to the conductivity of a uniform layer of gas of thickness equal to the local spacing, $\delta(r)$, consistent with the previous assumption of straight heat flow lines in the gaseous region. The local conductivity of the gaseous region is given by [8]:

$$k_g(r) = \frac{k_o}{1 + \alpha\beta\Lambda/\delta(r)} \tag{7}$$

where $k_o$ is the conductivity of the gas under continuum conditions at S.T.P., and $\alpha$ the accommodation parameter is defined as follows:

$$\alpha = 2\left(\frac{2-\alpha_1}{\alpha_1}\right) \tag{8}$$

where $\alpha_1$ is the accommodation coefficient, and $\beta$ is defined by:

$$\beta = \frac{1}{P_r}\left(\frac{2\gamma}{\gamma+1}\right) \tag{9}$$

$\gamma$ being the ratio of specific heats, and Pr is the Prandtl number. The mean free path, $\Lambda$, is given in terms of the mean free path at S.T.P., $\Lambda_o$, as:

$$\Lambda = \Lambda_o\left(\frac{T}{T_o}\right)\left(\frac{P_o}{P}\right) \tag{10}$$

The local spacing for two spheres in elastic contact is given by the following [12]:

$$\delta(r) = 2\left[\sqrt{(D/2)^2 - a^2} - \sqrt{(D/2)^2 - r^2} + \frac{2a^2}{\pi D}\left[(2 - (r/D)^2)\sin^{-1}(a/r) + \sqrt{(r/a)^2 - 1} - \pi/2\right]\right] \tag{11}$$

The local temperature difference, $\Delta T(r)$, is taken as the average of the following two cases: (i) The temperature distribution on the gas-solid interface is induced by the heat flow through the solid-solid contact under vacuum conditions. This was used by Yovanovich in his coupled model [11]. The local temperature difference for this model is given by the following expression:

$$\Delta T_1(r) = \left(\frac{2\Delta T_a}{\pi}\right)\tan^{-1}\sqrt{(r/a)^2 - 1} \tag{12}$$

(ii) The temperature distribution on the gas-solid interface is induced by parallel heat flow through the gas as well as the solid. This was used by Kunii and Smith [6] and Kaganer [8]. Incorporating the local variation in the gaseous conductivity given by Eq. (7), the following expression for local temperature difference is obtained:

$$\Delta T_2(r) = \frac{\Delta T_a}{(D/\delta(r)-1)k_g(r)/k_s+1} \tag{13}$$

The actual temperature distribution is somewhere between the two above. Since $\Delta T_1(r)$ and $\Delta T_2(r)$ do not differ substantially, the average is taken to yield:

$$\Delta T(r) = \frac{\Delta T_a}{2}\left[(2/\pi)\tan^{-1}\sqrt{(r/a)^2 - 1} + \frac{1}{(D/\delta(r)-1)k_g(r)/k_s + 1}\right] \tag{14}$$

Substituting Eqs. (7), (11), 14), and Eq. (6) into Eq. (5) and defining the effective gas conductivity in a similar manner to the solid effective conductivity (i.e. based upon a cubic cell of side D), there results [15]:

$$k_{ge} = \frac{k_o}{L} I \tag{15}$$

where the integral is defined as

$$I = \int_1^{\zeta} I_n \, dx \tag{16}$$

and the integrand is

$$I_n = \frac{x \tan^{-1}\sqrt{x^2-1}}{\delta^*(x) + ML} + \frac{(\pi/2)x}{(k_o/k_s)[2L-\delta^*(x)] + [\delta^*(x)+ML]} \tag{17}$$

The non-dimensional parameters are defined as follows:

$$x = r/a; \quad \zeta^* = \zeta/r; \quad \delta^*(x) = \delta(r)/a \tag{18}$$

and the modified Knudsen number is

$$M = 2\alpha\beta\Lambda/D \tag{19}$$

The value of the integral was obtained numerically [15].

The integral $I_n$ may be viewed as a non-dimensional heat flow per unit length in the radial direction, r. Fig. 2 shows the variation of $I_n$, as given by Eq. (17), with the parameter M.

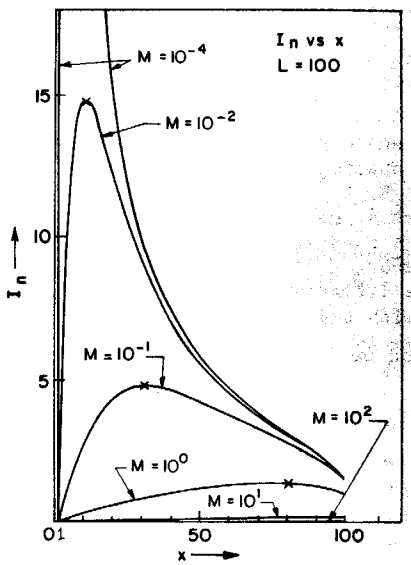


Fig. 2 Local variation of heat flow per unit length of radius.

For small M, corresponding to relatively high gas pressures, the main contribution to I is due to a very small region in the vicinity of the contact. This is observed in Fig. 2 where $I_n$ reaches a maximum value when x is small. For this case, the gas conduction is of relative importance compared with solid conduction. At large values of M, $I_n$ decreases and flattens suggesting that the entire gas

region contributes approximately equally to the overall gaseous heat flow, I; but this occurs at lower gas pressures where the solid conduction dominates the heat transfer. This observation suggests that the conduction through the interstitial gas of variable thickness should be modelled as constriction heat flow through a small gas region associated with each contact.

Figure (3) compares the effective gaseous conductivity obtained from Eq. (15) with the conductivity obtained from an analysis by Kaganer [8], in which the conductivity of the gas was evaluated at the constant spacing of 2D/3. The present model improves upon the previous analysis by allowing for the region where the gas is rarefied ($M \leq 10^{-1}$) to move towards the contact area (x=1) with increasing gas pressure. This results in a monotonic increase in conductivity over a very wide range of M. It differs substantially from the behaviour of a uniform gas layer of 2D/3 thickness, in which the variation of $k^*_{ge}$ is more rapid in the range $10^{-2} < M < 10^{1}$ and furthermore does not allow for increase in the gaseous conductivity beyond a value of M approximately equal to $10^{-2}$, Fig. 3.

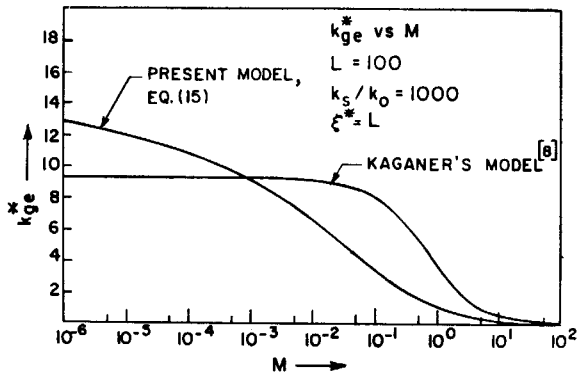


Fig. 3 Comparison between the present model and one employing a constant local gas spacing (Kaganer [8])

Figures 4 and 5 demonstrate the effect of the solid to gas conductivity ratio, $k_s/k_o$, and the sphere to contact diameter ratio, L. Because the temperature difference across the gaseous region decreases with the ratio $k_s/k_o$, the $k^*_{ge}$ curves do not collapse into one, which would mean that $k_{ge}$ is directly proportional to $k_o$. The effective gas

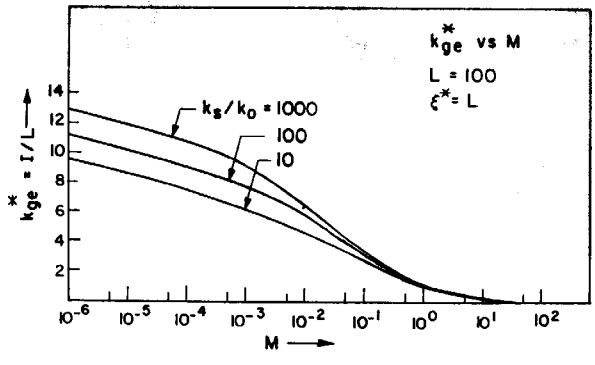


Fig. 4 Effect of solid to gas conductivity ratio, $k_s/k_o$, on effective gas conductivity

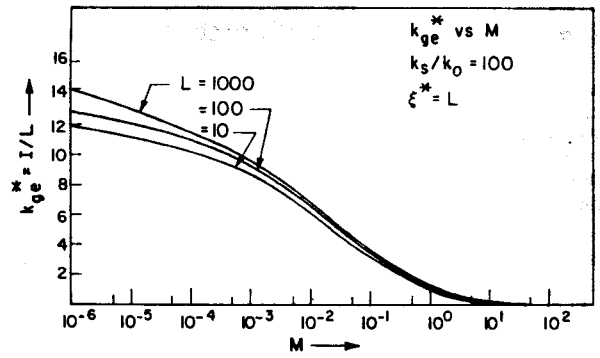


Fig. 5 Effect of sphere to contact diameter ratio, L, on effective gas conductivity

conductivity $k^*_{ge}$ at small values of M is larger than unity because the relatively highly conducting solid allows the heat to flow through the very thin gas region adjacent to the contact area. The effective gaseous conductivity increases with a decrease in the contact to sphere diameter ratio because the maximum value of $I_n$ increases and moves inward.

Since the solid and gaseous effective conductivities were based on the same cell dimensions and are thermally in parallel the overall effective conductivity, $k_e$, is simply the sum of the two, and therefore,

$$k_e = k_{se} + k_{ge} = \frac{1}{L}(k_s + k_o I) \qquad (20)$$

## B. Basic Cells

Simple cubic packing (CP), body-centered close packing (BCC), and face-centered close packing (FCC) are particular examples of regularly packed spheres. These three packings are chosen as the subject of consideration, although other regular packings with intermediate contact numbers and solid fractions, $\rho$, exist.

Analysis of basic cells representing CP, BCC, and FCC packings was presented by Chan and Tien [14]. Their analysis considered evacuated beds only, and, furthermore, only a single orientation of each packing with respect to the macroscopic temperature gradient. Figures 6a, 6b, and 6c correspond to CP, BCC, and FCC basic cells, respectively. These basic cells represent the particular orientation of each packing, here designated orientation A, where the macroscopic temperature gradient is in the z direction.

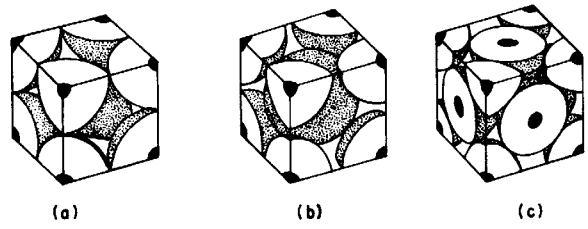


Fig. 6 Basic cells of CP, BCC and FCC packings in orientation A

Three such orientations, A, B, and C, for the three packings under consideration, are shown in

Figs. 7a, 7b, and 7c, respectively. The direction cosines of the macroscopic temperature gradients are (0, 0, 1), ($\sqrt{2}/2$, $\sqrt{2}/2$, 0) and ($\sqrt{3}/3$, $\sqrt{3}/3$, $\sqrt{3}/3$), respectively. These orientations enable the construction of basic cells which consist of two parallel isotherms and perpendicular adiabats.

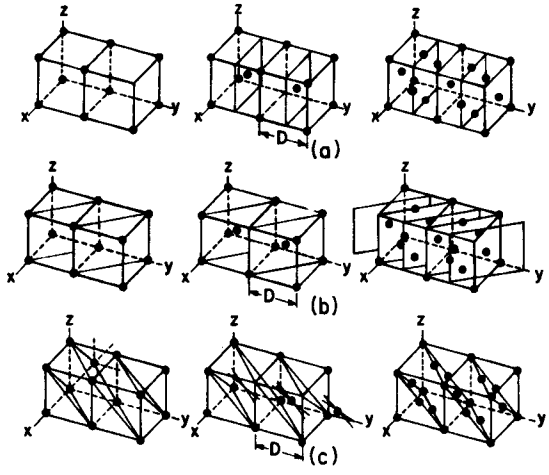


Fig. 7 Three orientations, A, B and C for packings CP, BCC and FCC

An example of a cell at an orientation different from A is shown in Fig. 8. This cell represents an FCC packing in orientation C, denoted FCC(C). The two horizontal boundaries are at uniform temperatures, $T_1$ and $T_2$, while the six vertical boundaries are adiabatic.

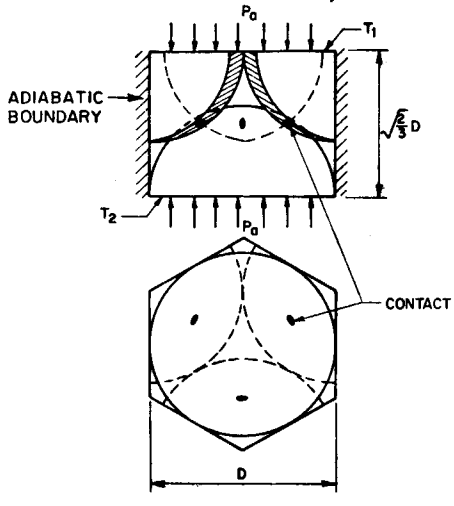


Fig. 8 FCC(C) basic cell

Each basic cell consists of a number of contact regions, each encompassing a circular solid-solid contact and an associated volume of gas of a particular shape, depending upon the specific packing structure encountered. The heat flow lines within each gas region become increasingly perpendicular to each contact plane as the solid-solid contact area is approached. Since the major gaseous contribution to the heat flow occurs relatively near the solid-solid contact, the area through which the gaseous heat flow occurs is transformed into an equivalent circular area, and, in addition, the heat flow lines are assumed to be perpendicular to the contact plane. With this simplification, the problem of heat conduction in a basic cell can be solved directly in terms of the results presented earlier for a single contact region.

The analysis of a basic cell proceeds as follows:

(i) the apparent pressure, $P_a$, on a basic cell is related through geometry, to the normal load, N, on a contact. The Hertz relation, Eq. (2), is used to calculate the sphere to contact diameter ratio, L, as follows:

$$L = \frac{F_1}{[3P_a(1-\nu^2)/E]^{1/3}} \tag{21}$$

where $F_1$ is obtained from the geometry of the basic cell alone. Defining:

$$\Delta = \frac{1}{[3P_a(1-\nu^2)/E]^{1/3}} \tag{22}$$

L may then be written as:

$$L = F_1\Delta \tag{23}$$

(ii) the gaseous region area is transformed to a circular one, and its radius, $\zeta^*$, is evaluated, resulting in:

$$\zeta^* = F_3\Delta \tag{24}$$

The gaseous region area is found by dividing the sphere surface area by the number of participating contacts. It should be noted that contacts perpendicular to the macroscopic temperature field do not participate in conduction and therefore are not considered.

(iii) the overall resistance, $R_t$, is determined from the thermal resistance network for each basic cell, and

(iv) the apparent conductivity of a basic cell, $k_a$, is obtained incorporating the overall dimensions, i.e., the height, h, and the area, A, and is written as follows [15]:

$$k_a = \frac{F_2}{\Delta}[k_s + k_o I(M,\Delta,k_s/k_o,F_1,F_3)] \tag{25}$$

The procedure was employed successively for each of the basic cells (except BCC(C)), and the results are summarized in Table 1.

Table 1: $F_1$, $F_2$, and $F_3$ for various basic cells

| Basic cell (ρ) | Orientation | $F_1$ | $F_2$ | $F_3$ |
|---|---|---|---|---|
| CP(0.524) | A | 1 | 1 | 1.00 |
| | B | 1 | 1 | 0.87 |
| | C | 1 | 1 | 0.75 |
| BCC(0.680) | A | $3^{1/6}$ | $3^{1/3}$ | 0.79 |
| | B | $3^{1/6}$ | $3^{1/3}$ | 1.04 |
| | C* | -- | -- | -- |
| FCC(0.740) | A | $2^{1/2}$ | 2 | 0.94 |
| | B | $2^{1/2}$ | 2 | 0.85 |
| | C | $2^{1/2}$ | 2 | 1.05 |

*not analyzed due to difficulty in constructing a thermal basic cell.

## C. Regularly Packed Spheres

The above analysis yielded apparent thermal conductivities for three discrete solid fractions, $\rho = 0.524, 0.680, 0.740$. The dependency of the apparent conductivity on the various packings and orientations is manifested through the three constants $F_1$, $F_2$ and $F_3$. In the light of the relatively small range of $F_3$, and its weak influence on the gaseous conduction, one may use an overall average value of $F_3$ ($\bar{F}_3 = 0.91$) for all packings and orientations. Hence the packings are nearly isotropic and only the constants $F_1$ and $F_2$ are required to evaluate the apparent conductivity.

The apparent conductivity of regularly packed spheres with intermediate solid fractions may be evaluated by interpolation of the results of the three discrete solid fractions. Second order polynomials were fitted to the values of $F_1$ and $F_2$ given in Table 1, yielding:

$$F_1(\rho) = 10.53\rho^2 - 11.39\rho + 4.077 \qquad (26)$$

and

$$F_2(\rho) = 29.95\rho^2 - 33.22\rho + 10.18 \qquad (27)$$

The above functional relations for $F_1$ and $F_2$ in terms of the solid fraction in conjunction with Eq. (25) provide the means of determining the apparent conductivity of regularly packed spheres with corresponding solid fraction $\rho$.

## Experimental Results and Discussion

### A. Sphere-flat Contact Region

Experimental data for a sphere-flat contact region were obtained by Kitscha and Yovanovich [13] for varying mechanical load and gas pressure, for air and argon. For a sphere-flat contact region, a special case of the model presented, here, one can determine,

(i) The contact radius

$$a = [(3/4)ND(1-\nu^2)/E]^{1/3} \qquad (28)$$

and, (ii) the non-dimensional local spacing:

$$\delta^*(x) = \sqrt{L^2-1} - \sqrt{L^2-x^2} + \frac{2}{\pi L}[(2-x^2)\sin^{-1}(1/x) + \sqrt{x^2-1} - (\pi/2)] \qquad (29)$$

A small radiative contribution to the overall heat transfer was observed during the test program. To account for their heat transfer, the following thermal resistance was added in parallel to the gaseous and solid conduction resistances:

$$R_r = \frac{1}{4\varepsilon_1 A_1 F_{12} \sigma T_m^3} \qquad (30)$$

where $\varepsilon_1$, $A_1$, $F_{12}$ $\sigma$, and $T_m$ are the emissivity, projected surface area, radiative view factor, Stefan-Boltzman constant, and mean temperature, respectively. Free convection was demonstrated to be negligible and is not considered in the present model.

The experimental and theoretically calculated values are presented in Figs. 9 and 10. The agreement is excellent except for relatively small loads, when L = 115 for air and argon. The discrepancy is believed due to experimental error. Such results demonstrate that the effect of the mechanical load and gas properties are well modelled by the present analysis.

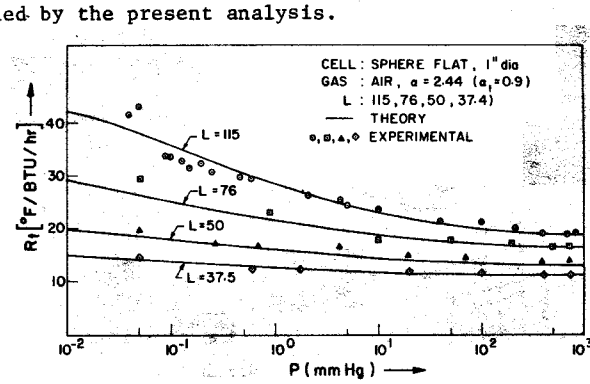


Fig. 9 Thermal resistance of a sphere-flat contact region with air at various loads and gas pressures

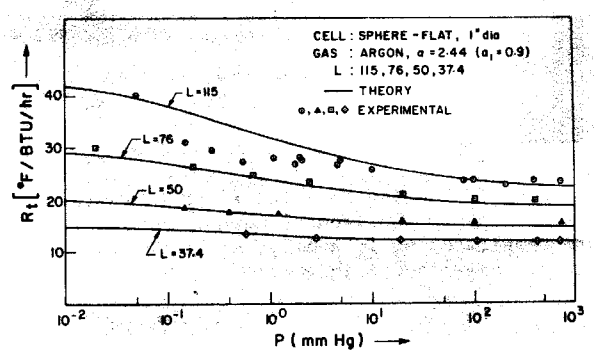


Fig. 10 Thermal resistance of a sphere-flat contact region with argon at various loads and gas pressures

### B. FCC(C) Basic Model

An FCC(C) basic cell, shown in Fig. 8, was constructed using 1.25" diameter steel balls. The cell was placed between two coaxial rods of corresponding cross section, Fig. 11. The rods were axially loaded with dead weights to ensure equal loads on three contacts. Such an arrangement eliminates the experimental difficulty encountered due to thermal stresses associated with linkages. The power was supplied by Joulean heating, and the heat flow through the cell was determined by measuring the temperature gradient on the sink side of the cell. Multilayer insulation was used to render the side walls effectively adiabatic.

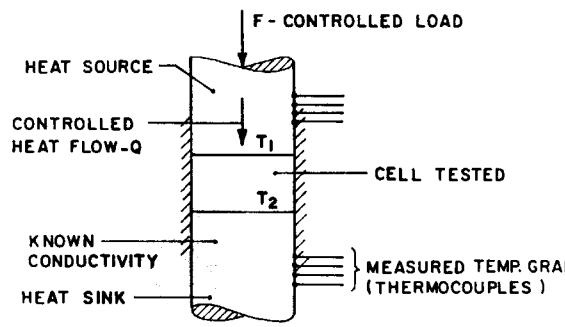


Fig. 11 Experimental set-up of a basic cell

The entire assembly was placed in a controlled pressure environment. Low vacuums ($10^{-2}$ to 1mm Hg) were obtained by establishing pressure equilibrium with a bleeder valve and constant evacuation by a mechanical vacuum pump. This technique eliminated the difficulty encountered in maintaining a constant pressure due to unavoidable air leakage into the system. This is believed to have caused the discrepencies observed in the sphere-flat experimental data [13] when L = 115.

By applying successively larger loads, the small radiant contribution to thermal resistance was effectively defined.

The theoretical and experimental values of total resistance under vacuum conditions for various loads are compared in Fig. 12.

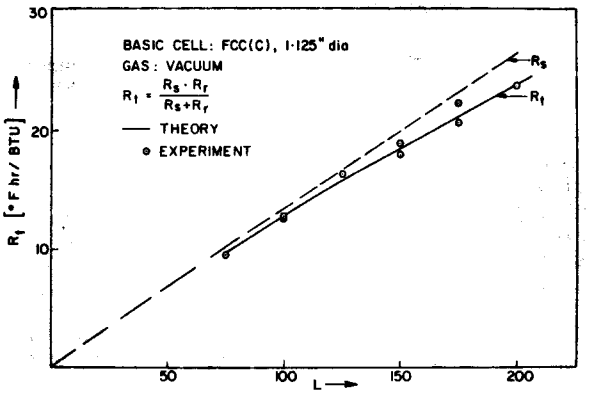


Fig. 12 Thermal resistance of an FCC(C) cell versus mechanical load in vacuum

Figures 13 and 14 show the theoretical and experimental total thermal resistances for air and helium respectively. The gas pressure ranged from $10^{-1}$ to 740 mm Hg. The accommodation coefficients were chosen to fit the test data at the lightest mechanical load. The values for air and helium were 0.9 and 0.4 respectively, which is in good agreement with values reported in the literature.

The solid thermal resistance varies linearly with L as seen in Fig. 12. The experimental results for thermal resistance span a substantial load range ($75 \leq L \leq 200$). The excellent agreement of the experimental results with the predicted values (incorporating radiation) over the entire range effectively verifies the effect of load in the present theoretical results as given by Eq. (3).

The total thermal resistance varies gradually over a wide range of M, as seen in Figs. 13 and 14. It continues to do so beyond $M=10^{-2}$ (corresponding to $P \simeq 1.5$ mm Hg for air, and $p \simeq 5$ mm for helium). This trend is not predicted by the previous models, which did not allow for local variation in gas conductivity (see Fig. 3). The experimental total resistance varies substantially from vacuum to atmospheric pressure, particularly at large values of L. In light of the excellent agreement over the entire range of gas pressure (or M) the present model for gaseous contribution to the overall thermal resistance is effectively demonstrated.

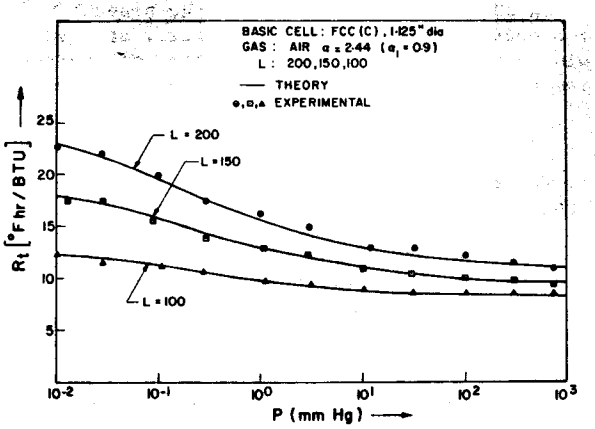


Fig. 13 Thermal resistance of an FCC(C) cell with air as a function of load and gas pressure

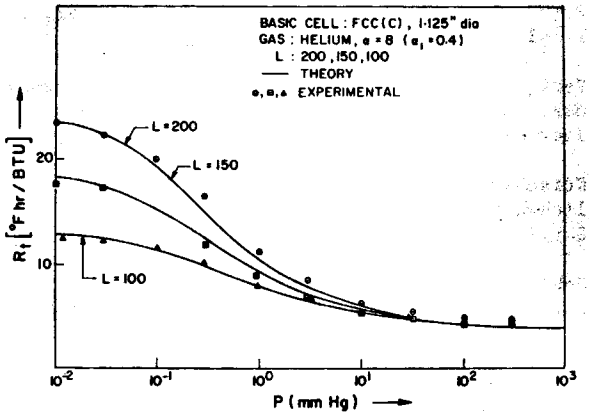


Fig. 14 Thermal resistance of an FCC(C) cell with helium as a function of load and gas pressure

The solid to gas conductivity ratio, $k_s/k_o$, is difficult for air and helium (approximately 1800 and 300 respectively). The good agreement for both packing demonstrates that its effect is well accounted for by the present thermal model. It might be noted, though, that the values of $k_s/k_o$ in both cases are relatively large which is a necessary condition for application of the present constriction model.

## Summary

Analytical results for the apparent conductivity of regularly packed spheres were obtained. The analysis incorporates the effects of mechanical load, gas pressure, packing, solid to gas conductivity ratio and other properties of the solid and the gas successfully. The results differ markedly from previous ones particularly in the effect of gas pressure upon the gaseous contribution to the overall conductivity. The excellent agreement of the present analysis with experimental data obtained with basic cells indicates an improvement upon previous models in so far as regularly packed spheres are concerned. It is believed that future work, based on these results, incorporating additional parameters associated with random packed beds should be successful.

In addition we may add that the present model for a contact region could be directly applied to a wide variety of problems consisting of contacts between curved surfaces submerged in a stagnant gas.

## Acknowledgements

The authors acknowledge the financial support of the National Research Council. One of the authors (Y. Ogniewicz) thanks the National Research Council for an NRC scholarship. The advice and assistance of R. Kaptein during the experimental work are gratefully acknowledged.

## References

[1] Beveridge, G.S.G. and Haughey, D.P., "Axial Heat Transfer in Packed Beds, Stagnant Beds Between 20 and 750°C", Int. J. Heat Mass Transfer, 14, 1092-1113 (1971).

[2] Luikov, A.V., et al, "Thermal Conductivity of Porous Systems", Int. J. Heat Mass Transfer, 11, 117-140 (1968).

[3] Yagi, S. and Kunii, D., "Studies on Heat Transfer Near Wall Surface in Packed Beds", A.I.Ch.E. Journal, 6, No. 1, 97-104 (1960).

[4] Krischer, O. and Kroll, K., "Die Wissenschaftlichen Grundlager der Trochnungstechnik", Bd. 1, Berlin-Gottingen-Heidelberg (1956).

[5] Schotte, W., "Thermal Conductivities of Porous Solids", A.I.Ch.E. Journal, 6, No. 1, 63-67 (1960).

[6] Kunii, D. and Smith, J.M., "Heat Transfer Characteristics of Porous Rocks", A.I.Ch.E. Journal, 6, No. 1, 71-78 (1960).

[7] Masamune, S. and Smith, J.M., "Thermal Conductivity of Spherical Particles", Ind. Eng. Chem. Fund., 2, 136-143 (1963).

[8] Kaganer, B.M.G., Thermal Insulation in Cryogenic Engineering, Translated from Russian by Moscona, A., Israel Program for Scientific Translation, Jerusalem (1969).

[9] Wakao, N. and Vortmeyer, D., "Pressure Dependency of Effective Conductivity of Packed Beds, Chem. Eng. Sci., 26, 1753-1765 (1971).

[10] Wakao, N. and Kato, K., "Effective Thermal Conductivity of Packed Beds", J. Ch. E. of Japan, 2, No. 1, 24-33 (1969).

[11] Yovanovich, M.M. and Kitscha, W.W., "Modeling the Effect of Air and Oil Upon the Thermal Resistance of a Sphere-Flat Contact", AIAA No. 73-746 (1973). Thermophysics and Spacecraft Thermal Control, Prog. Aeronautics and Astronautics, Vol. 35, Editor, R.G. Hering, MIT Press, pp. 293-319 (1974).

[12] Cameron, A., Principles of Lubrication, John Wiley and Sons, Inc., New York, N.Y. (1966).

[13] Kitscha, W.W. and Yovanovich, M.M., "Experimental Investigation on the Overall Thermal Resistance of Sphere-Flat Contacts", AIAA, No. 74-113 (1974). Heat Transfer with Thermal Control Applications, Prog. Aeronautics and Astronautics, Vol. 39, Editor, M.M. Yovanovich, MIT Press, pp. 93-110 (1975).

[14] Chan, C.K. and Tien, C.L., "Conductance of Packed Spheres in Vacuum", J. Heat Transfer, 95, 302-308 (1973).

[15] Ogniewicz, Y., "Conduction in Basic Cells of Packed Beds", M.A.Sc. Thesis, Department of Mechanical Engineering, University of Waterloo, (1975).